

Comparison of the AlN and GaN crystalline quality on 2-inch silicon substrate via two growth methods

Yangfeng Li*, Chak Wah Tang, Kei May Lau*

Department of Electronic and Computer Engineering, The Hong Kong University of Science and Technology, Clear Water Bay, Kowloon, Hong Kong

ARTICLE INFO

Communicated by T. Paskova

Keywords:

- A1. GaN on Si
- A2. Prewflow TMAI
- A2. Nitridation
- B1. Dislocation density
- B2. Photoluminescence
- B3. TEM

ABSTRACT

The crystalline quality of aluminum nitride (AlN) and gallium nitride (GaN) has been investigated through two growth methods on 350 μm [1 1 1]-orientation 2-inch silicon substrates. One method employs nitridation with ammonia prior to the growth of a medium temperature AlN layer. The other method is to preflow trimethyl aluminum (TMAI) prior to the growth of a low temperature AlN layer. The growth parameters are the optimized ones under each growth conditions. The thickness of the GaN layer is adjusted to keep the total thickness of the epilayers unchanged. According to the X-ray diffraction (XRD) rocking curves, with preflow TMAI, both the AlN and GaN present fewer dislocation densities. Reciprocal space maps show that with preflow TMAI treatment, the tensile stress is alleviated both in the AlN and GaN layers. With three layers of indium gallium nitride (InGaN) quantum dots separated by GaN barriers added on the as-grown GaN layer, the sample undergone preflow TMAI has more superb photoluminescence performances of both GaN and InGaN than those of the other one. The root-mean-square surface roughness value obtained by atomic force microscopy is larger in the sample with preflow TMAI treatment. It was due to the a little overlong preflow TMAI time. The transmission electron microscopy (TEM) shows the sample undergone preflow TMAI treatment has fewer defects and abrupt interface between AlN and silicon substrate.

1. Introduction

Growing gallium nitride (GaN) on silicon (Si) substrates has attracted much attention of researchers because the silicon substrate is cost-effective, easy to get large size and promising to integrate photonic devices with integration circuits [1–4]. However, the values of mismatch of lattice parameter and thermal expansion coefficient between GaN and Si are rather high. Thus, the crystalline quality of GaN grown on Si is relatively poor and easy to crack due to the large tensile stress caused by the large mismatch [5–7]. To alleviate the large tensile strain in the GaN layer, an aluminum nitride (AlN) nucleation layer is always inserted between the GaN and Si [8]. The AlN intermediate layer also plays an important role in suppressing the meltback etching problem when GaN was grown directly on Si substrate [9]. Additionally, the Si substrate usually needs some pre-treatment prior to the growth of AlN [10].

Some researchers prefer to use ammonia (NH_3) to nitridize the Si surface to form a nitrogen atomic layer just as the growth of GaN on sapphire substrates [11–13]. Wu-Yih Uen et al. [14] introduced the NH_3 to nitridate the Si(1 1 1) surface in metal organic chemical vapor deposition (MOCVD) system under different temperatures (viz. 750 $^\circ\text{C}$,

950 $^\circ\text{C}$, 1120 $^\circ\text{C}$) and attained the hexagonal GaN of best crystalline quality with the full-width at half-maximum (FWHM) value of GaN (0 0 2) plane of 0.279 $^\circ$ (1004.4 arcsec) from X-ray diffraction (XRD) rocking curve, while the root-mean-square (RMS) roughness was 5.057 nm. Mohd Nazri Abd. Rahman et al. studied the effects of the nitridation time on the crystalline quality of GaN on Si (1 1 1) substrate and attained the best GaN with the FWHMs of (0 0 2) and (1 0 2) of 1126 and 2012 arcsec, respectively [15]. Abdul Kadir et al. [12] reported a FWHM of (0 0 2) of \sim 550 arcsec of a 1 μm -thick GaN grown on 200 mm Si substrate by using the AlN nucleation layer and step-graded AlGaIn interlayers under the nitridation time of 16 s. While other researchers insist that the nitridation of the Si introduce Si_xN_x complexes resulting in the deterioration of the crystalline quality of the epilayer [10,16–20]. Franky Lumbantoruan et al. [16] reported the high quality GaN grown on Si (1 1 1) substrate by optimizing the TMAI-preflow time. C.C. Huang et al. [5] introduced AlGaIn step-graded intermediate layers after the AlN layer grown on the TMAI pre-dosed Si substrate and achieved a 2 μm GaN layer with the XRD FWHM of 690 arcsec. A.P. Lange et al. [18] investigated the surface morphology and surface elements and proposed a Al-Si liquid solution phase transform mechanism during the AlN nucleation process on the Si. And they have

* Corresponding authors.

E-mail addresses: eyyangfeng@ust.hk (Y. Li), ekmlau@ust.hk (K.M. Lau).

<https://doi.org/10.1016/j.jcrysgr.2020.125545>

Received 12 October 2019; Received in revised form 29 January 2020; Accepted 8 February 2020

Available online 10 February 2020

0022-0248/ © 2020 Elsevier B.V. All rights reserved.

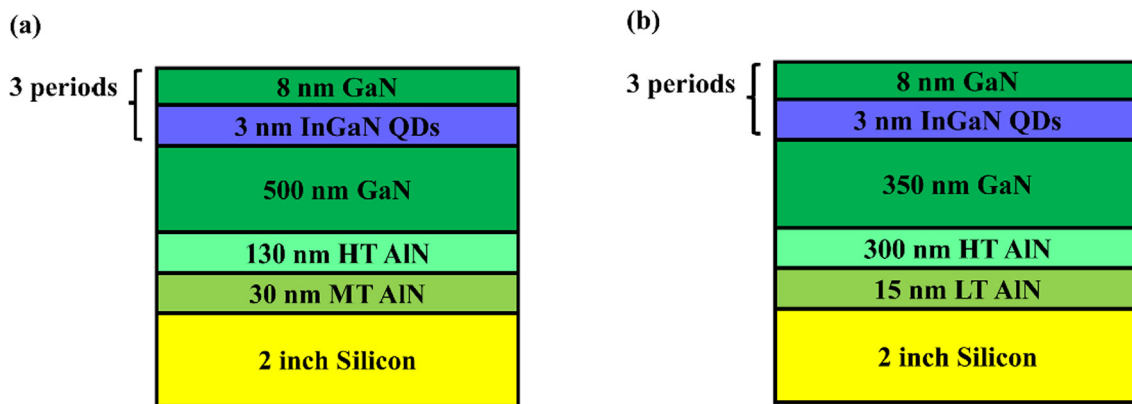


Fig. 1. Schematic diagram of the cross-sectional structure of samples (a) A and (b) B. (For interpretation of the references to colour in this figure legend, the reader is referred to the web version of this article.)

also reported that by preflow TMAl, the crystalline quality of AlN will be improved [17]. Nevertheless, the comparison of these two methods are rare to be reported. And most of the GaN grown on Si are rather thick (the total underlayer thickness usually thicker than 1 μm) in the research papers. In general, the thicker the GaN layer is, the fewer dislocation densities are there, as most of the dislocations will annihilate within a few hundred nanometers of GaN growth [9]. Furthermore, the AlGaIn interlayers will also significantly improve the crystalline quality of the subsequently grown GaN layer [10]. However, if we want to achieve the micro-disk laser devices, the total underlayer thickness need to be reduced, e.g., to 650 nm [21,22], and the AlGaIn interlayers are almost impossible to be inserted in such structures. As the thickness of the micro-disk increases, the modes along the vertical direction will increase thus reducing the spontaneous emission coupling factor, resulting in a high threshold of the micro-disk laser [23,24]. As the laser is dislocation sensitive [25], growing the thin GaN with high quality on Si substrate becomes an urgent issue.

In this study, we investigate the crystalline quality of the AlN and GaN epilayer by using two growth methods. One method uses ammonia to nitridize the Si substrate, and the other uses trimethyl aluminium (TMAl) to treat the Si substrate before the growth of the AlN nucleation layer. The crystalline quality of AlN and GaN was evaluated by XRD rocking curves and the screw and edge dislocation densities were extracted from the values of XRD FWHM through some models fabricated by other researchers. Three pairs of indium gallium nitride (InGaIn) [$\text{In}_{0.2}\text{Ga}_{0.8}\text{N}(3\text{ nm})/\text{GaN}(8\text{ nm})$] multiple quantum dots (MQDs) layers were added on the as-grown GaN layer. The photoluminescence (PL) spectra of GaN and MQDs and the surface and interface morphology were investigated. Such a structure was designed to get micro-disk laser of InGaIn QDs on Si, the lasing results of which will be presented in the future work.

2. Experimental section

We fabricated two samples labeled A and B by using the AXITRON 6×2 -inch close-coupled showerhead metal organic chemical vapor deposition (MOCVD) system. The substrates were 350 μm 2-inch silicon with a [1 1 1]-oriented surface. There were normally no offcut angles in the silicon substrates. The substrates were at first exposed in H_2 ambient for 10 min at 1050 $^\circ\text{C}$ then treated with silane for another 10 min at the same temperature to desorb the surface contaminants. After desorption, sample A was nitridized by NH_3 with a flow rate of 300 sccm for 16 s at 990 $^\circ\text{C}$. Then, a 30-nm-thick medium-temperature AlN (MT-AlN) layer was deposited at the same temperature. Prior to the growth of a 500-nm-thick GaN layer at 1050 $^\circ\text{C}$, a high temperature AlN (HT-AlN) layer with a thickness of 130 nm was deposited at 1100 $^\circ\text{C}$. While Sample B was treated by preflow TMAl with a flow rate of

7.36 $\mu\text{mol}/\text{min}$ at 760 $^\circ\text{C}$ for 3 min. Then a low-temperature AlN (LT-AlN) layer with a thickness of 15 nm was deposited at 920 $^\circ\text{C}$ followed by a HT-AlN layer with a thickness of 300 nm at 1100 $^\circ\text{C}$. To ensure the total thickness of the epilayer holding unchanged, the thickness of the subsequently deposited GaN layer was reduced to 350 nm under the same growth conditions as those of sample A. After the GaN growth, three pairs of InGaIn MQDs [$\text{In}_{0.2}\text{Ga}_{0.8}\text{N}(3\text{ nm})/\text{GaN}(8\text{ nm})$] were deposited on the as-grown GaN layer both of samples A and B. The QDs were fabricated by a growth interruption technique with a 15 s post-growth annealing after the growth of each QDs layer. The growth temperature of the InGaIn MQDs was 680 $^\circ\text{C}$ [26]. All the samples were crack-free after the growth except about 1–2 mm in the edge region. The crystalline quality was characterized by using high resolution X-ray diffraction (HRXRD) with a PANalytical system equipped with a four-bounce channel-cut Ge (2 2 0) monochromator that delivered a pure $\text{CuK}\alpha 1$ line of 1.5406 \AA . The reciprocal space maps (RSMs) were also measured by the same XRD apparatus with an asymmetric scan geometry. The atomic force microscope (AFM) with a tapping mode was performed to investigate the surface morphology. A continuous-wavelength He-Cd laser emitting at 325 nm was performed to measure the room temperature PL of the InGaIn MQDs. The PL of GaN was also measured with the 325 nm laser from 50 K to 120 K. The transmission electron microscopy (TEM) was employed to investigate the interface morphology and dislocation densities.

3. Results and discussion

The schematic structures of samples A and B are shown in Fig. 1(a) and (b), respectively. The growth parameters of the structure of A and B have been optimized previously. Then the samples A and B are compared under each other's optimized growth conditions.

Fig. 2 shows the in-situ monitor curves of reflectivity of a 633 nm laser, together with the wafer true temperature curves during the growth process of samples A and B. The values of reflectivity of A and B are comparable. The growth temperature of both samples was also well controlled during the growth process. The thickness of the HT-AlN layer was calculated from the reflectivity curves with a refractive index of 2.15. The exact thickness values of the HT-AlN layer are 137 nm and 314 nm for samples A and B, respectively. The thicknesses of the GaN layer are 476 nm and 388 nm for samples A and B, respectively, calculated with a refractive index of 2.38. The experimental results coincide well with the structure parameters we designed in Fig. 1.

HRXRD rocking curves are performed to evaluate the crystalline quality of the AlN and GaN layers of samples A and B. Fig. 3(a) and (c) show the rocking curves of (0 0 2), (0 0 4) and (0 0 6) crystalline planes of samples A and B for AlN and GaN, respectively. Sample B presents narrower FWHM values and stronger diffraction intensity than those of sample A both for AlN and GaN, indicating the better crystalline quality

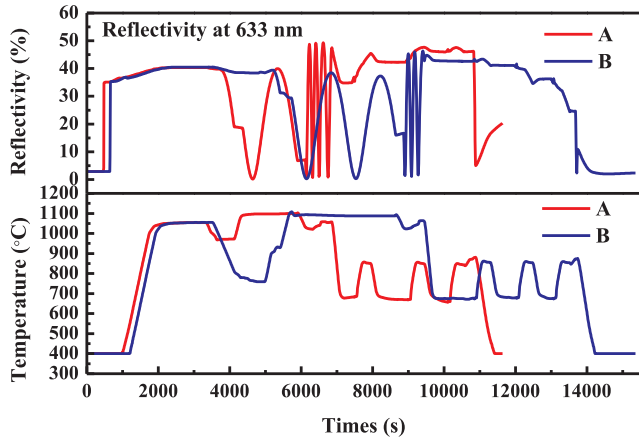


Fig. 2. The in-situ monitor curves of (top) reflectivity, and (bottom) wafer true temperature during the growth process of samples A and B. (For interpretation of the references to colour in this figure legend, the reader is referred to the web version of this article.)

of AlN and GaN in sample B. The relatively thicker AlN layer in sample B is suspected to contribute to the narrowing of the FWHM and the increasing of the diffraction intensity. However, although the GaN layer in sample B is thinner than that in sample A, it has a narrower FWHM value and stronger diffraction intensity than those in sample A. Thus, we attribute the narrowing of the FWHM and the enhancement of diffraction intensity mainly to the improved crystalline quality of AlN and GaN in sample B. The values of the (0 0 2) FWHM for AlN and GaN of sample A are 1536 and 856 arcsec, respectively. While those of sample B are 813 and 619 arcsec, respectively. The FWHM of AlN (0 0 2) obtained in this work is smaller than that (0.43°) in the latest report [27].

Although the thickness of GaN in sample B is only 388 nm, the FWHM of GaN (0 0 2) is also comparable with the value (562.8 arcsec) reported recently, where the thickness of GaN was 2 μm [28]. The rocking curves were fitted by the Pseudo-Voigt function, from which the FWHM and index n of the rocking curve were extracted [29]. Then, we use the Williamson-Hall (W-H) plot to obtain the tilt angle, which refers to the screw dislocation density in the crystalline films [30]. The equation can be written as

$$(FWHM \times q)^n = (\omega_{\text{tilt}} \times q)^n + \left(\frac{1}{L_{\parallel}}\right)^n, \quad (1)$$

where q is equal to $\sin\theta/\lambda$, θ is the Bragg reflection angle, λ is the wavelength of the incident X-ray, ω_{tilt} is the angle indicating the density of the screw dislocation, and L_{\parallel} refers to the lateral coherence length. n is the parameter extracted from the Pseudo-Voigt function fitting process. The values of n for AlN are 1.27 and 1.31 for samples A and B, respectively. The fitted results with Eq. (1) are presented in Fig. 3(b). The values of the tilt angle (ω_{tilt}) are 0.42° and 0.20° for samples A and B, respectively. The density of the screw dislocation was calculated by using equation $N_s = \frac{\omega_{\text{tilt}}^2}{4.35b_s^2}$ [31,32], where N_s is the density of the screw dislocation and b_s is the length of the Burgers vector, which is equal to the lattice parameter of c_{AlN} . The values of the screw dislocation density are $5.03 \times 10^9 \text{ cm}^{-2}$ and $1.18 \times 10^9 \text{ cm}^{-2}$ for the AlN layer in samples A and B, respectively. The values of the tilt angle of the GaN layer are 0.23° and 0.17° for samples A and B, respectively, obtained by similar analysis methods. The linear fitting results are presented in Fig. 3(d). The screw dislocation densities of GaN are $1.40 \times 10^9 \text{ cm}^{-2}$ and $7.41 \times 10^8 \text{ cm}^{-2}$ for samples A and B, respectively. The density of the screw dislocation in sample B is half of that in sample A.

The twist angle (ω_{twist}) indicates the density of the edge dislocation. However, the exact twist angle is generally difficult to be obtained

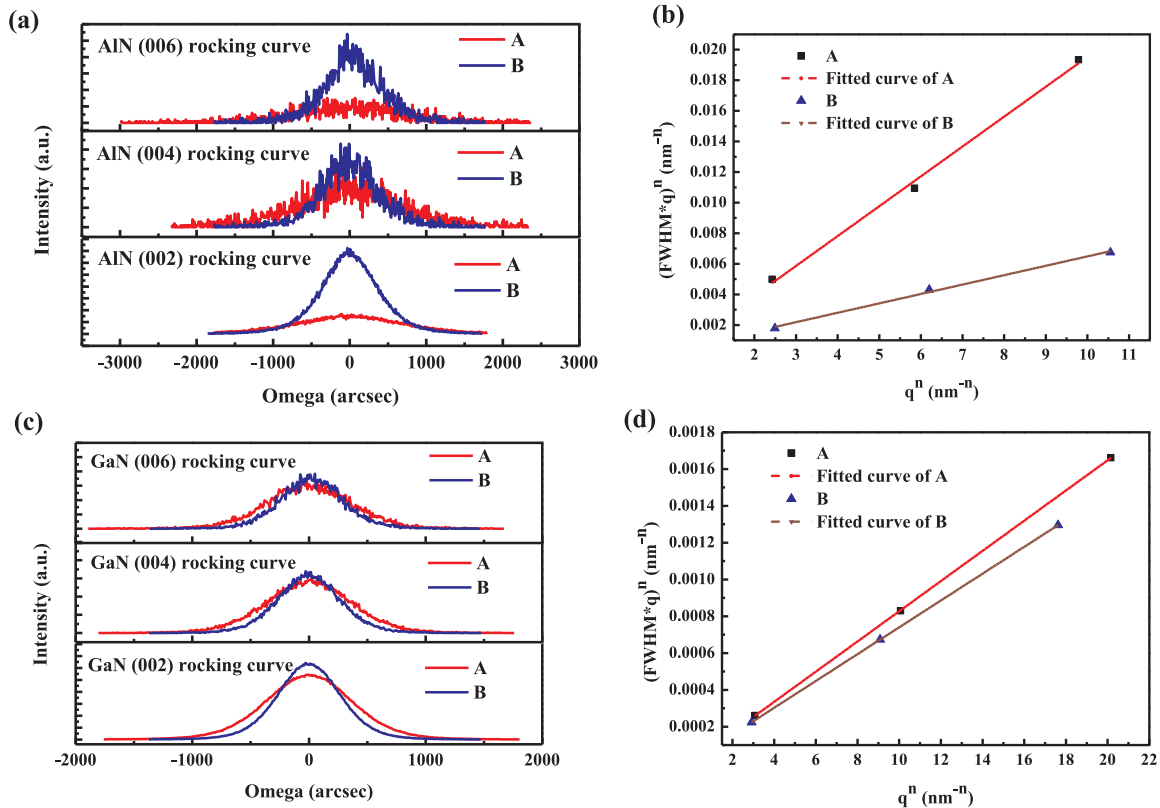


Fig. 3. (a) (0 0 2), (0 0 4) and (0 0 6) rocking curves for AlN of samples A and B. (b) W-H plots for AlN of samples A and B. (c) Rocking curves of the (0 0 2), (0 0 4) and (0 0 6) planes for GaN of samples A and B. (d) W-H plots for GaN of samples A and B. (For interpretation of the references to colour in this figure legend, the reader is referred to the web version of this article.)

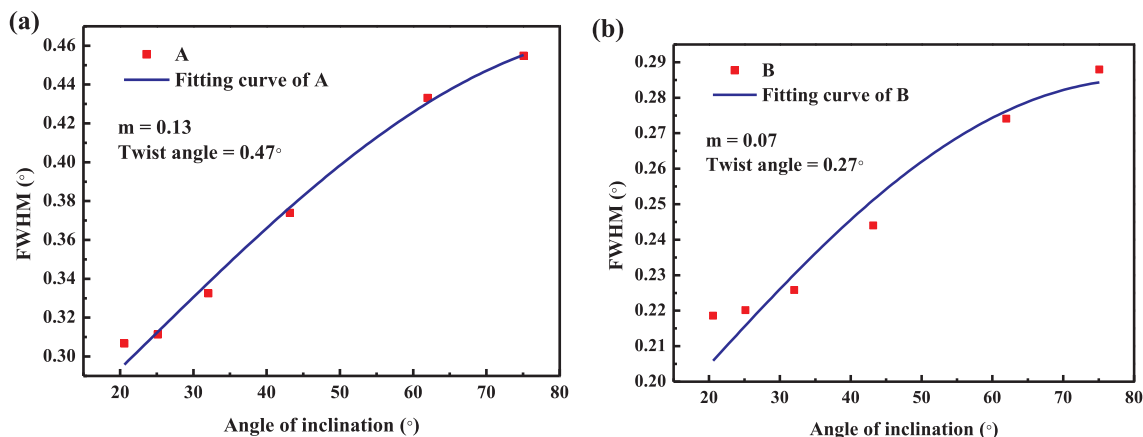


Fig. 4. The FWHM as a function of the inclination angle between the diffraction plane and the surface plane. The blue solid line is the fitted curve through the model proposed by Srikant *et al.* (a) and (b) show the experimental data and the fitting curve of samples A and B, respectively. (For interpretation of the references to colour in this figure legend, the reader is referred to the web version of this article.)

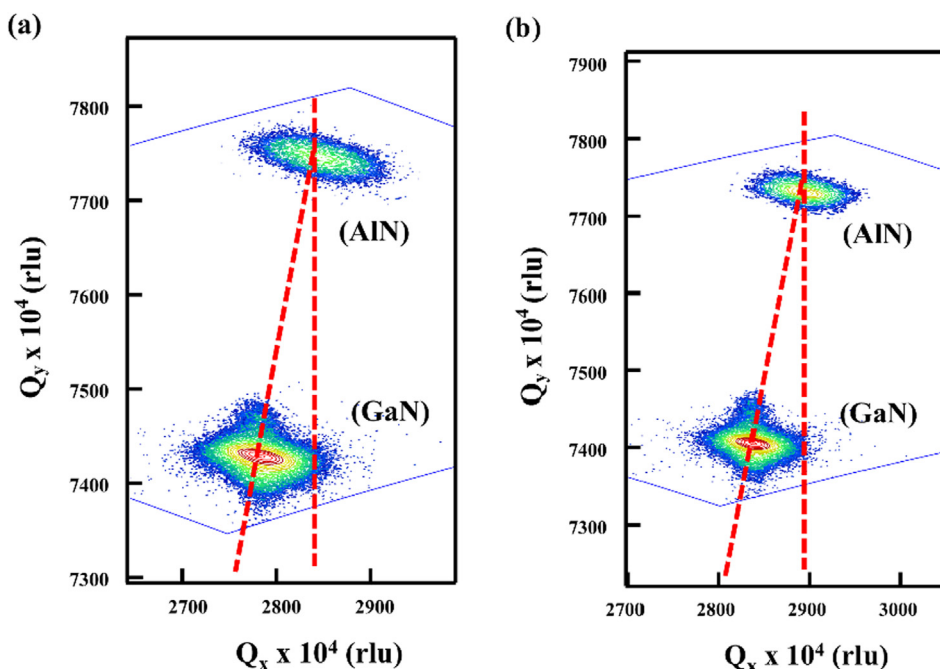


Fig. 5. The (1 0 5) RSM for AlN and GaN of samples (a) A and (b) B. The red-dotted lines are the guidelines indicating the relaxation between the GaN and AlN layers. (For interpretation of the references to colour in this figure legend, the reader is referred to the web version of this article.)

directly from XRD measurement due to the slender thickness of the epilayer. Here, the skew symmetric geometry for $(h k l)$ reflections of GaN with different inclination angles was applied, namely the skew rocking curves of the (1 0 1), (1 0 2), (1 0 3), (1 0 4), (1 0 5), and (2 0 1) planes were obtained. The inclination angle refers to the angle between the measured crystalline plane and the sample surface plane. The value of the FWHM of GaN (1 0 2) of sample B is 864 arcsec, which is also comparable with the value (794.5 arcsec) of a 2- μ m-thick GaN layer from the latest report [28]. While the value of FWHM of GaN (1 0 2) of sample A is 1286 arcsec. The curves were fitted by the Pseudo-Voigt function and the average values of n were 1.37 and 1.40 for samples A and B, respectively. The curves of the FWHM changing with inclination angle were fitted by a model proposed by Srikant *et al.* [29] and are shown in Fig. 4(a) and (b) for samples A and B, respectively. The parameter m refers to the dependence between the tilt and twist angles. If m is larger than 0, it means the interaction between the tilt and twist angle is anti-correlated. The values of the twist angle calculated by the aforementioned fitting model are 0.47° and 0.27° for samples A and B,

respectively. Then the density of the edge dislocation can be obtained through the equation $N_e = \frac{\omega_{twist}^2}{4.35b_e^2}$ [31,32], where N_e is the density of the edge dislocation, ω_{twist} is the twist angle and b_e is the length of the Burgers vector. The edge dislocation densities are $1.51 \times 10^{10} \text{ cm}^{-2}$ and $5.08 \times 10^9 \text{ cm}^{-2}$ for samples A and B, respectively. According to the XRD measurement results, the density of the edge dislocation in sample B has been reduced to 33.6% of that in sample A.

To evaluate the relaxation between the AlN and GaN layers in the two samples, an asymmetric RSM scan for samples A and B was carried out. Fig. 5(a) and (b) show the (1 0 5) plane RSM for the AlN and GaN layers of samples A and B, respectively. The values of the strain relaxation degree between the GaN and AlN layer are 44% and 47% in samples A and B, respectively [33]. During the growth process, a little more stress was released in sample B than that in sample A. It is worth noting that in sample B, both AlN and GaN present larger Q_x values, noting the in-plane compressive stress in sample B is larger than that in sample A [10]. It is well known that a large tensile stress is the main reason for the deterioration in crystalline quality of GaN when grown

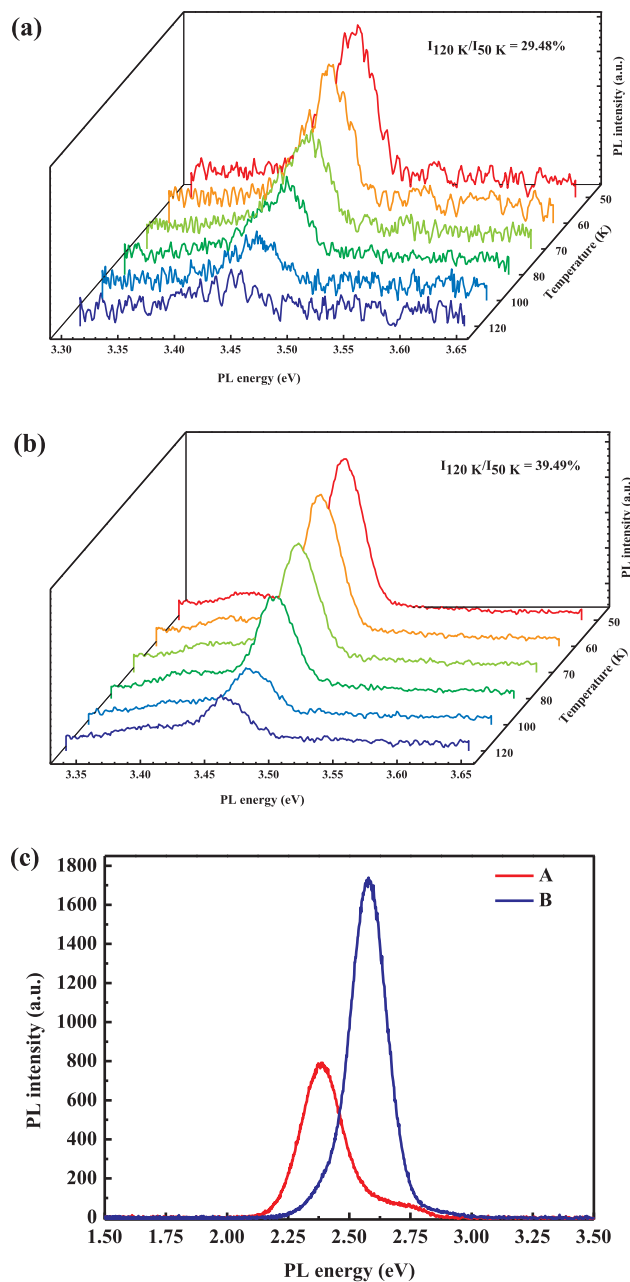


Fig. 6. (a) The PL spectra of GaN from 50 K to 120 K of samples A and (b) B. (c) The room temperature PL spectra of InGaN QDs of samples A and B. (For interpretation of the references to colour in this figure legend, the reader is referred to the web version of this article.)

on Si substrate. The insertion of an AlN layer aims to alleviate the tensile stress by introducing compressive stress between the AlN and GaN layer. According to the RSM results, sample B suffers less tensile strain than sample A.

As most of the defects in GaN are recognized as non-radiative recombination centers, which will significantly exacerbate the PL property of GaN. The GaN PL spectra from 50 K to 120 K of A and B are shown in Fig. 6(a) and (b), respectively. The peaks locating at ~ 3.45 eV recognized as the GaN near-band-edge emission are clear to be seen in both samples [34]. The PL intensity of GaN of sample A decreases rapidly with the increasing temperature and the PL peak becomes hardly to be distinguished from the background signal when the temperature over 120 K. While the PL peak of sample B is still distinguishable above 120 K (the spectra at the temperature above 120 K are not shown

here.). By fitting the peaks with the Gaussian function, we calculated the ratio of the PL integral intensity at 120 K to that at 50 K. The ratio value of A is 29.48% while that of B is 39.49%. The PL intensity of sample A decays more rapidly with rising temperature than that of sample B, indicating severer non-radiative recombination processes in the GaN layer of sample A. Furthermore, sample B presents a narrower FWHM at 50 K of 32.19 meV than that of A of 46.71 meV. As three pairs of InGaN QDs were deposited on the GaN template, room temperature PL spectra of the InGaN QDs for samples A and B are shown in Fig. 6(c). Although the wafer true temperatures were controlled to around 680 °C during the growth process of both samples, there exists a large red-shift of the peak energy in sample A. This may be due to the difference in wafer deformation during the growth process of the two samples. The exact reason needs to be further investigated. According to the PL spectra, sample B has a sharp peak with more than a two-fold enhanced PL intensity and a narrower FWHM (18.63 meV) than that (21.21 meV) of sample A. Combining the PL results, we conclude the optical performances of both GaN and InGaN QDs of sample B are superior to those of sample A.

The surface morphology of samples A and B is shown in Fig. 7(a) and (b), respectively. Sample A has a smoother surface with an RMS surface roughness of 0.620 nm for a scan area of $5 \mu\text{m} \times 5 \mu\text{m}$. While in sample B, the RMS value is 1.737 nm. As reported by other researchers [35–37], an overlong preflow TMAI time will exacerbate the surface morphology and deteriorate the crystalline quality. In our case, the TMAI preflow time is as long as 3 min, which may be a little overlong. To verify such an assumption, we fabricated another sample (labelled C) using the same growth conditions as sample B except with a 90-second TMAI preflow time. The RMS of sample C is reduced to 0.503 nm, whereas the (0 0 2) FWHM of GaN of C is increased to 741 arcsec. As we fabricated such structures aiming to get micro-disk lasers, the surface of which needn't be so much smooth. Whereas, the performance of micro-disk lasers is more sensitive to the dislocation density [25]. Sample B presents more than half reduced dislocation densities than those of sample A. We conclude the growth method of sample B is superior to that of sample A.

To further investigate the mechanism of the two growth methods, we grinded the two samples and then thinned them by ion milling. The cross-sectional TEM images shown in Fig. 8(a) and (b) were taken under 200 kV. From the TEM images, one can clearly distinguish the silicon substrate, the AlN layer, the GaN and the InGaN MQDs layers. Such regions are also labelled in Fig. 8(a) and (b). It is worth noting that the density of defects in AlN of sample A is rather large while that in sample B is reduced drastically. In sample A, a large number of defects emerge from the interface between the Si substrate and AlN, then they will partly annihilate and/or bend during the growth of AlN. However, the interface in sample B presents fewer defects, thus improving the crystalline quality of AlN. Judging from the TEM results, one can reasonably attribute the reduction of defects to the TMAI preflow treatment of the Si surface. With TMAI preflow treatment, the interface produces fewer defects thus reducing the dislocation density in the subsequently grown AlN and GaN layer. The mechanism of the TMAI preflow on reducing the dislocation density could be explained by the model proposed by A.P. Lange et al. [18]. According to their research, they found the Si surface will form Al-Si liquid alloy when it is undergone TMAI preflow treatment. The liquid alloy forms AlN islands and Si-rich patches when subsequently reacts with ammonia. Such a surface morphology will play a role in enhancing the dislocation bending during the growth process, thus leading to a AlN layer with fewer defects [17].

4. Conclusions

The crystalline quality of the AlN and GaN grown on 2-inch silicon substrate via two different growth methods was investigated. By treating with preflow TMAI, using a LT-AlN nucleation layer and a relatively thicker HT-AlN layer, we found the crystalline qualities of both

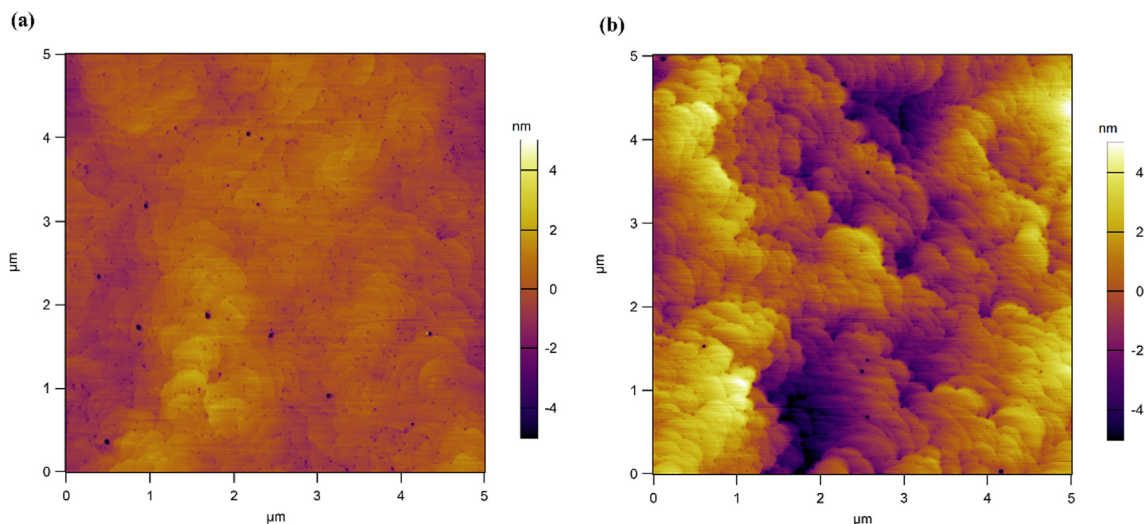


Fig. 7. AFM images of (a) sample A and (b) sample B, with a scan area of $5 \mu\text{m} \times 5 \mu\text{m}$. (For interpretation of the references to colour in this figure legend, the reader is referred to the web version of this article.)

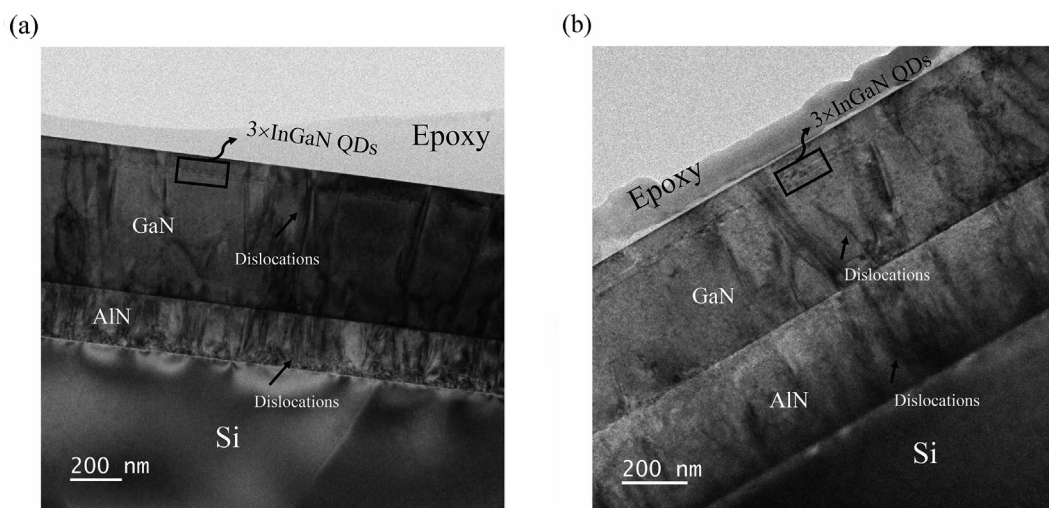


Fig. 8. The cross-sectional TEM images of samples A (a) and B (b), respectively.

AlN and GaN were significantly improved. The quantitative values of the density of the screw and edge dislocation in the AlN and GaN for samples A and B were calculated from the HRXRD rocking curves through theoretical models. Sample B presents lower densities of screw and edge dislocation both in the AlN and GaN layers. The RSM results show alleviated tensile stress and a larger relaxation degree between the GaN and AlN in sample B. An active layer comprised of three pairs of InGaN QDs was deposited on the GaN layer expected for achieving micro-disk lasers. Sample B has a stronger PL intensity and narrower FWHM of both GaN bulk layer and InGaN MQDs than those of sample A. The AFM images show a smoother surface of sample A, which is due to the a little overlong TMAI preflow time in sample B. However, we assume the surface status of sample B has fewer effects on exacerbating the performance of micro-disk laser devices. The TEM images show fewer defects between the AlN and Si interface of sample B, which is attributed to the TMAI-preflow effect. From the aforementioned results, we confirm that the growth method of sample B is superior to that of sample A.

CRediT authorship contribution statement

Yangfeng Li: Conceptualization, Methodology, Validation, Formal

analysis, Investigation, Data curation, Writing - original draft, Writing - review & editing, Visualization. Chak Wah Tang: Resources. Kei May Lau: Supervision, Resources.

Declaration of Competing Interest

The authors declare that they have no known competing financial interests or personal relationships that could have appeared to influence the work reported in this paper.

References

- [1] P. Lin, S. Huang, W. Wang, C. Chen, B. Chung, D. Wu, Appl. Surf. Sci. 362 (2016) 434, <https://doi.org/10.1016/j.apsusc.2015.11.226>.
- [2] A. Hu, C. Song, X. Yang, X. He, B. Shen, X. Guo, Nanotechnology 30 (2019) 314002, <https://doi.org/10.1088/1361-6528/ab1948>.
- [3] F. Iucolano, T. Boles, Mater. Sci. Semicond. Process 98 (2019) 100, <https://doi.org/10.1016/j.mssp.2019.03.032>.
- [4] Y. Ni, L. Li, L. He, T. Que, Z. Liu, L. He, Z. Wu, Y. Liu, Superlattices Microstruct. 120 (2018) 720, <https://doi.org/10.1016/j.spmi.2018.06.012>.
- [5] C.C. Huang, S.J. Chang, R.W. Chuang, J.C. Lin, Y.C. Cheng, W.J. Lin, Appl. Surf. Sci. 256 (2010) 6367, <https://doi.org/10.1016/j.apsusc.2010.04.018>.
- [6] Y. Li, W. Wang, Y. Lin, X. Li, L. Huang, Y. Zheng, Z. Zhang, G. Li, Mater. Lett. 207 (2017) 133, <https://doi.org/10.1016/j.matlet.2017.07.065>.
- [7] M. Suzuki, A. Nakamura, Y. Nakano, M. Sugiyama, J. Cryst. Growth 464 (2017)

- 148, <https://doi.org/10.1016/j.jcrysgro.2016.12.090>.
- [8] L. Pan, X. Dong, Z. Li, W. Luo, J. Ni, Appl. Surf. Sci. 447 (2018) 512, <https://doi.org/10.1016/j.apsusc.2018.04.001>.
- [9] A. Dadgar, et al., J. Cryst. Growth 248 (2003) 556, [https://doi.org/10.1016/S0022-0248\(02\)01894-8](https://doi.org/10.1016/S0022-0248(02)01894-8).
- [10] Y. Yang, et al., J. Cryst. Growth 376 (2013) 23, <https://doi.org/10.1016/j.jcrysgro.2013.04.043>.
- [11] E. Arslan, Ö. Duygulu, A.A. Kaya, A. Teke, S. Özçelik, E. Ozbay, Superlattices Microsc. 46 (2009) 846, <https://doi.org/10.1016/j.spmi.2009.09.009>.
- [12] A. Kadir, S. Srivastava, Z. Li, K.E.K. Lee, W.A. Sasangka, S. Gradecak, S.J. Chua, E.A. Fitzgerald, Thin Solid Films 663 (2018) 73, <https://doi.org/10.1016/j.tsf.2018.08.011>.
- [13] A. Wierzbicka, et al., Nanotechnology 24 (2013) 035703, <https://doi.org/10.1088/0957-4484/24/3/035703>.
- [14] W.-Y. Uen, Z.-Y. Li, S.-M. Lan, S.-M. Liao, J. Cryst. Growth 280 (2005) 335–340, <https://doi.org/10.1016/j.jcrysgro.2005.03.084>.
- [15] M.N.A. Rahman, Y. Yusuf, M. Mansor, A. Shuhaimi, Appl. Surf. Sci. 362 (2016) 572–576, <https://doi.org/10.1016/j.apsusc.2015.10.226>.
- [16] F. Lumbantoruan, Y.-Y. Wong, Y.-H. Wu, W.-C. Huang, N.M. Shrestha, T.T. Luong, T.B. Tinh, E.Y. Chang, Investigation of TMAI preflow to the properties of AlN and GaN film grown on Si(111) by MOCVD, 2014 IEEE International Conference on Semiconductor Electronics (ICSE2014), IEEE, Kuala Lumpur, Malaysia, 2014, pp. 20–23.
- [17] A.P. Lange, S. Mahajan, J. Cryst. Growth 511 (2019) 106, <https://doi.org/10.1016/j.jcrysgro.2019.01.040>.
- [18] A.P. Lange, X.L. Tan, C.S. Fadley, S. Mahajan, Acta Mater. 115 (2016) 94, <https://doi.org/10.1016/j.actamat.2016.05.036>.
- [19] K.Y. Zang, L.S. Wang, S.J. Chua, C.V. Thompson, J. Cryst. Growth 268 (2004) 515, <https://doi.org/10.1016/j.jcrysgro.2004.04.083>.
- [20] Y.-T. Fang, Y. Jiang, Z. Deng, P. Zuo, H. Chen, Chin. Phys. Lett. 31 (2014) 028101, <https://doi.org/10.1088/0256-307x/31/2/028101>.
- [21] M. Athanasiou, R. Smith, B. Liu, T. Wang, Sci. Rep. 4 (2014) 7250, <https://doi.org/10.1038/srep07250>.
- [22] M. Athanasiou, R.M. Smith, J. Pugh, Y. Gong, M.J. Cryan, T. Wang, Sci. Rep. 7 (2017) 10086, <https://doi.org/10.1038/s41598-017-10712-4>.
- [23] M.K. Chin, D.Y. Chu, S.T. Ho, J. Appl. Phys. 75 (1994) 3302–3307, <https://doi.org/10.1063/1.356137>.
- [24] Y. Zhang, X. Zhang, K.H. Li, Y.F. Cheung, C. Feng, H.W. Choi, Phys. Status Solidi A 212 (2015) 960–973, <https://doi.org/10.1002/pssa.201431745>.
- [25] H.A.R. El-Ella, F. Rol, M.J. Kappers, K.J. Russell, E.L. Hu, R.A. Oliver, App. Phys. Lett. 98 (2011) 131909, <https://doi.org/10.1063/1.3567545>.
- [26] Y. Li, Z. Jin, Y. Han, C. Zhao, J. Huang, C.W. Tang, J. Wang, K.M. Lau, Mater. Res. Express 7 (2019) 015903, <https://doi.org/10.1088/2053-1591/ab5be0>.
- [27] L. Huang, Y. Li, W. Wang, X. Li, Y. Zheng, H. Wang, Z. Zhang, G. Li, Appl. Surf. Sci. 435 (2018) 163, <https://doi.org/10.1016/j.apsusc.2017.11.002>.
- [28] J.C. Lin, S.J. Huang, Y.K. Su, C.H. Lai, Appl. Surf. Sci. 354 (2015) 148, <https://doi.org/10.1016/j.apsusc.2015.03.034>.
- [29] V. Srikant, J.S. Speck, D.R. Clarke, J. Appl. Phys. 82 (1997) 4286, <https://doi.org/10.1063/1.366235>.
- [30] R. Chierchia, T. Böttcher, H. Heinke, S. Einfeldt, S. Figge, D. Hommel, J. Appl. Phys. 93 (2003) 8918, <https://doi.org/10.1063/1.1571217>.
- [31] P. Gay, P.B. Hirsch, A. Kelly, Acta Cryst. 7 (1954) 41, <https://doi.org/10.1107/S0365110X54000060>.
- [32] C.G. Dunn, E.F. Kogh, Acta Metallurgica 5 (1957) 548, [https://doi.org/10.1016/0001-6160\(57\)90122-0](https://doi.org/10.1016/0001-6160(57)90122-0).
- [33] S. Pereira, M.R. Correia, E. Pereira, K.P. O'Donnell, E. Alves, A.D. Sequeira, N. Franco, I.M. Watson, C.J. Deatcher, Appl. Phys. Lett. 80 (2002) 3913, <https://doi.org/10.1063/1.1481786>.
- [34] J.F. Muth, J.H. Lee, I.K. Shmagin, R.M. Kolbas, H.C. Casey, B.P. Keller, U.K. Mishra, S.P. DenBaars, Appl. Phys. Lett. 71 (1997) 2572, <https://doi.org/10.1063/1.120191>.
- [35] J. Cao, S. Li, G. Fan, Y. Zhang, S. Zheng, Y. Yin, J. Huang, J. Su, J. Cryst. Growth 312 (2010) 2044, <https://doi.org/10.1016/j.jcrysgro.2010.03.032>.
- [36] K. Matsumoto, T. Ono, Y. Honda, S. Murakami, M. Kushimoto, H. Amano, Jpn. J. Appl. Phys. 57 (2018) 091001, <https://doi.org/10.7567/jjap.57.091001>.
- [37] H. Jia, Y. Chen, X. Sun, D. Li, H. Song, H. Jiang, G. Miao, Z. Li, Chin. J. Lumines. 33 (2012) 83, <https://doi.org/10.3788/fgxb20123301.0082>.